PHYSICAL REVIEW B VOLUME 52, NUMBER 5 1 AUGUST 1995-I

^{63,65}Cu NMR and NQR study of the Cu^{2+} electronic state and the spin dynamics in the spin-Peierls compound CuGeO$_3$

Masayuki Itoh and Shinji Hirashima
Department of Physics, Faculty of Science, Chiba University, Yayoi-cho, Inage-ku, Chiba 263, Japan

Kiyoichiro Motoya
Department of Physics, Faculty of Science and Technology, Science University of Tokyo, Yamazaki, Noda 278, Japan

(Received 23 January 1995)

^{63,65}Cu NMR and NQR measurements have been performed to study the Cu^{2+} electronic state and the spin dynamics in CuGeO$_3$, which is an inorganic compound that undergoes the spin-Peierls transition at $T_{\mathrm{sp}} \sim 14$ K. The NQR frequency is discussed in connection with the lattice dimerization accompanied by the spin-Peierls transition. The Knight shift with an axial symmetry showed the temperature dependence corresponding to the reduction of the spin susceptibility. From the analysis of the Knight shift and the magnetic susceptibility, orbital and spin susceptibilities are evaluated. The analysis of the hyperfine structure leads to a conclusion that the electronic state of the Cu^{2+} ion above T_{sp} is described by a single-ion model in a crystal field with a tetragonal symmetry. The supertransferred hyperfine interaction, which is one of the characteristic features of Cu^{2+} ions in the CuO$_2$ plane in the high-T_c superconducting copper oxides, is found not to play an important role in CuGeO$_3$. The temperature dependence of the nuclear spin-lattice relaxation rate $1/T_1$ clearly shows presence of a gap in the magnetic excitation spectrum below T_{sp}. The relaxation mechanism is discussed based on the spinless fermion treatment for an $S=\frac{1}{2}$ one-dimensional Heisenberg antiferromagnet (1DHAF) above T_{sp} and for a nonuniform $S=\frac{1}{2}$ 1DHAF with two unequal and alternating exchange interactions below T_{sp}. Above T_{sp}, it is also discussed in terms of the dynamical susceptibilty of the 1DHAF.

I. INTRODUCTION

One-dimensional Heisenberg antiferromagnets (1DHAF) have provided interesting magnetic phenomena such as the spin-Peierls (SP) transition,[1] the Haldane gap,[2] and so on. In particular, the 1DHAF of $S=\frac{1}{2}$ is known to have a singlet ground state. The lowest-lying excited state called the des Cloizeaux–Pearson mode is located with no energy gap at the zone center and the zone boundary.[3] If there exists a spin-phonon interaction in the $S=\frac{1}{2}$ 1DHAF, the spin and lattice dimerizations simultaneously take place at the SP transition temperature T_{sp}. Consequently, below T_{sp}, the dimerization produces an energy gap between the nonmagnetic total-spin singlet ground state and the lowest excited triplet state in the magnetic excitation spectrum. The SP transition had been reported only in the organic salts such as tetrathiafulvalene-CuS$_4$C$_4$(CF$_3$)$_4$ (TTF-CuBDT), TTF-AuBDT, and methylethylmorpholinium ditetracyanoquinodimethane [MEM-(TCNQ)$_2$].[1] Recently, Hase, Terasaki, and Uchinokura found a new inorganic SP compound CuGeO$_3$ with $T_{\mathrm{sp}} \sim 14$ K.[4] A number of experimental studies have been performed to clarify the SP transition in this compound.[5–15,18–25]

CuGeO$_3$ crystallizes in the orthorhombic structure with the space group *Pbmm* at room temperature.[16] A unit cell contains two elongated CuO$_6$ octahedra which form the edge-sharing Cu-O chains along the c axis. Magnetic susceptibility χ shows an abrupt reduction below ~ 14 K, and a broad maximum around ~ 56 K, indicating the low dimensionality.[4] However, the temperature dependence of χ above T_{sp} cannot be well explained by a theoretical curve with the exchange constant $J=88$ K numerically calculated by Bonner and Fisher[17] for the $S=\frac{1}{2}$ 1DHAF. The intrachain exchange constant $J_c \sim 10.4$ meV, the interchain exchange constants $J_b \sim 0.1J_c$ and $J_a \sim -0.01J_c$, and the energy gap 2.11 meV at $T=0$ K were obtained by an inelastic neutron-scattering experiment.[18] An appearance of an energy gap in the magnetic excitation spectrum below T_{sp} was indicated by the nuclear relaxation measurements.[19,20] Anisotropic g values were also determined by the ESR measurements.[21,22]

The lattice dimerization, which is one of the most characteristic features in the SP transition, had not been found for some time after the discovery of the SP transition in CuGeO$_3$. Recently, however, x-ray and elastic neutron-scattering measurements revealed a second-order structural transition to a dimerized ground state below T_{sp}.[23] In the electron-diffraction measurements,[24] a superlattice reflection with indices $(h/2,k,l/2)$ (h, k, and l are odd) was also found below T_{sp}. Furthermore, the Cu dimerization and oxygen displacements below T_{sp} were determined by a neutron-scattering measurement.[25] Therefore, an essential point in the mechanism of the SP transition in CuGeO$_3$ seems to be understood in the framework of a conventional theory of the SP transition based on the spin-phonon coupling. Nevertheless, the microscopic magnetic properties related with the low dimensionality and the SP transition have not been

0163-1829/95/52(5)/3410(11)/$06.00

clarified even in the static properties as well as in the dynamics.

To investigate microscopically the Cu^{2+} electronic state and the spin dynamics in CuGeO$_3$, we have performed ^{63,65}Cu NMR and NQR measurements. The change in the NQR frequency below T_{sp} is determined to probe the lattice dimerization. The anisotropic Knight shift will be discussed from the aspect of the local symmetry. Furthermore, the orbital susceptibility and the hyperfine structure are obtained by the analysis of the magnetic susceptibility and the Knight shift. Finally, from the temperature dependence of the nuclear spin-lattice relaxation rate $1/T_1$, the spin dynamics will be discussed for the 1DHAF with a uniform exchange interaction above T_{sp} and the two unequal alternating ones below T_{sp}.

II. EXPERIMENTAL PROCEDURE

A polycrystalline sample used in the present experiment was prepared by a solid-state reaction method. Appropriate mixtures of GeO$_2$ (5N) and CuO (4N) were ground and pressed into a pellet. It was fired at 950 °C in air for 7 days with several intermediate regrindings. The sample was confirmed to be a single phase by x-ray-diffraction analysis. Magnetic susceptibility and magnetization process were measured by using a SQUID magnetometer (Quantum Design, model MPMS). NMR measurements were performed by using a coherent spin-echo spectrometer with sweeping the magnetic field of a superconducting magnet. NQR spectra were taken point by point of frequency in zero external field using a superheterodyne coherent pulsed spectrometer. The nuclear spin-lattice relaxation time T_1 was measured for the Cu NQR signals by a saturation recovery method.

III. EXPERIMENTAL RESULTS

A. Magnetic susceptibility and magnetization curve

Figure 1 shows the temperature dependence of the magnetic susceptibility χ of CuGeO$_3$ taken at 5 T. Here, the susceptibility is defined by $\chi = M/H$, where M is the magnetization at a field H. The result is essentially the same as the previous data.[4] Below ~14 K, χ reduces exponentially with decreasing temperature. A slight upturn of χ below ~5 K, which approximately follows a relation $\chi = \chi_{\text{CW}} + \chi_0$, where χ_0 is a constant and the Curie-Weiss term $\chi_{\text{CW}} = C/(T - \Theta)$ with $C = (8.53 \pm 1.13) \times 10^{-5}$ emu K/mol and $\Theta = 1.1 \pm 1.2$ K is considered to be ascribed to the impurity local moments. The inset in Fig. 1 shows the result after subtracting the χ_{CW} part with a constant term from the experimental data. The temperature-independent susceptibility at low temperatures comes from orbital and diamagnetic contributions, which we will discuss later. The susceptibility shows a broad maximum at ~60 K, and gradually decreases with increasing temperature. This behavior cannot be well explained by the Bonner-Fisher calculation for the $S = \frac{1}{2}$ 1DHAF.[4]

Figure 2 shows the magnetization vs magnetic field curve up to 5.5 T in the SP phase of CuGeO$_3$. A slight upturn above ~4 T is seen in the temperature range 10–13 K because of the reduction of the SP energy gap with increasing temperature.

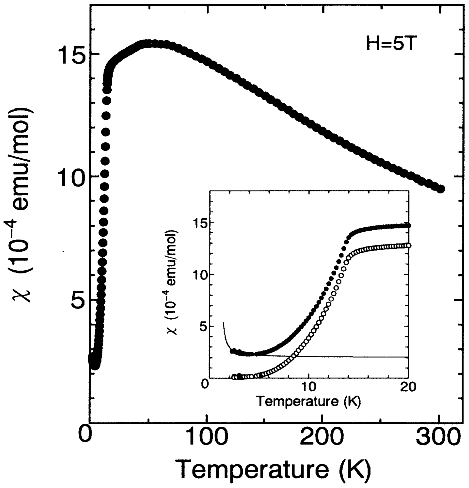

FIG. 1. Temperature dependence of the magnetic susceptibility of CuGeO$_3$ taken at 5 T. The susceptibility χ is defined by $\chi = M/H$ where M is the magnetization at a field H. The inset shows an expanded figure at low temperatures. The open circles represent the results after subtracting the Curie-Weiss (the solid curve) term due to the impurity local moments from the experimental data.

B. NQR spectrum

Two resonance lines were observed at about 34.2/31.7 MHz in zero external field in the temperature range 4.2–80 K. A spectrum taken at 4.2 K is shown in Fig. 3, which is in agreement with a previous report.[19] By the

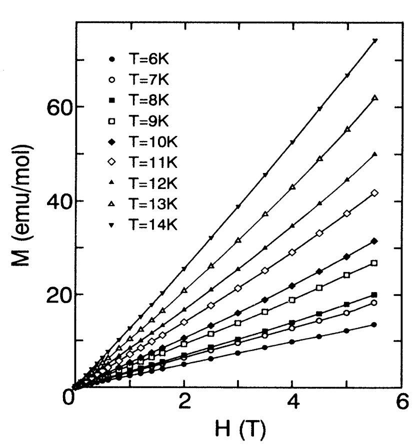

FIG. 2. Magnetization vs magnetic field at various temperatures below T_{sp} in CuGeO$_3$. The solid curves are drawn to guide the eye.

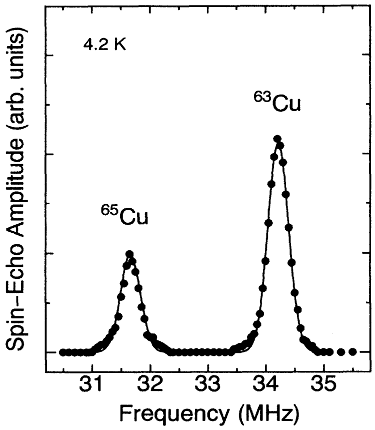

FIG. 3. ^{63}Cu and ^{65}Cu NQR spectra in CuGeO$_3$ at 4.2 K in zero external field. The solid curve is the result of least-squares fitting the data to two Gaussian functions.

least-squares-fitting procedure, the central frequencies and the line widths of the two Gaussian functions were determined to be 34.22±0.01/31.66±0.02 and 0.42±0.02/0.40±0.04 MHz at 4.2 K, respectively. The ratio of the frequency at the two peaks 1.081±0.01 is in excellent agreement with that of the nuclear quadrupole moment $^{63}Q/^{65}Q=1.081$.[26] Also the ratio of the signal intensity at 34.22 MHz to that at 31.66 MHz is 2.2, corresponding to that of the natural abundance of ^{63}Cu to ^{65}Cu. Thus, the two resonances are assigned to the ^{63}Cu/^{65}Cu NQR lines. As is presented in Fig. 4(a), the NQR frequency $^{63}\nu_{\mathrm{NQR}}$ is almost temperature independent in the temperature range 4.2–16 K.

C. NMR spectrum and Knight shift

Figure 5 shows a field-swept spin-echo spectrum taken at 4.2 K and 75.5 MHz. The observed powder pattern consists of a superposition of two equivalent spectra due to the ^{63}Cu and ^{65}Cu isotopes. Each spectrum is explained by taking into account the electric quadrupole and the Zeeman interactions. To extract the Knight shift from the spectra, we concentrate our attention to the pattern of the central $(+\frac{1}{2}\leftrightarrow-\frac{1}{2})$ transition as is presented in the inset of Fig. 5.

To determine the Knight shift, we assume that the X, Y, and Z principal axes of the Knight shift tensor are the same as those of the electric-field gradient (EFG) tensor. This assumption is usually reasonable because both tensors are mainly governed by the local symmetry of the Cu site. A powder pattern of the central transition has anomalies at five frequencies for resonance $\nu_1-\nu_5$ in a constant field (corresponding to H_1-H_5 in a constant frequency) as expressed in the Appendix where the quadrupole effect is treated by the second-order perturbation.[27] In the range of $0<\eta<\frac{1}{3}$ where the asymmetry parameter of the EFG tensor η is defined as $\eta=|V_{XX}-V_{YY}|/|V_{ZZ}|$ (V_{XX}, V_{YY}, and V_{ZZ} are the principal components of the EFG tensor and $|V_{XX}|\leq|V_{YY}|\leq|V_{ZZ}|$), two peaks appear at H_2 and H_4, two shoulders at H_1 and H_5, and a

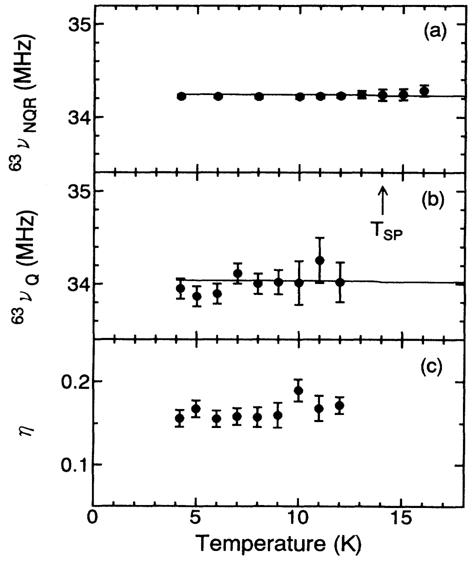

FIG. 4. Temperature dependence of (a) the ^{63}Cu NQR frequency $^{63}\nu_{\mathrm{NQR}}$, (b) the ^{63}Cu quadrupole frequency $^{63}\nu_Q$, and (c) the asymmetry parameter of the electric-field gradient tensor η in CuGeO$_3$. The solid curves are the results estimated based on a point charge model with taking into account the displacements of each ion accompanied by the SP transition (see the text).

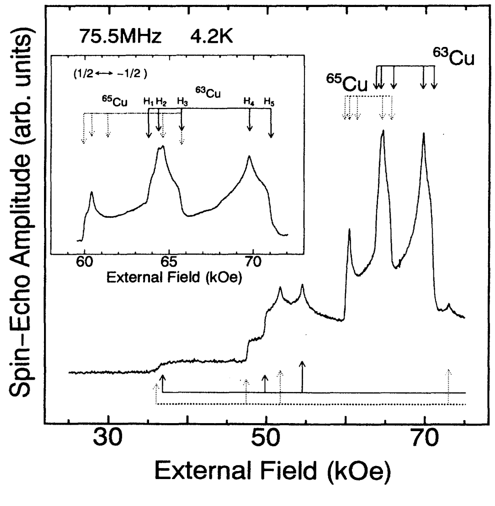

FIG. 5. ^{63}Cu and ^{65}Cu powder NMR spectra in CuGeO$_3$ taken at 4.2 K and 75.5 MHz. The solid and dotted arrows correspond to the central (downward) and satellite (upward) transition lines of the ^{63}Cu and ^{65}Cu spectra, respectively. The inset shows an expanded figure of the spectra of the central $(\frac{1}{2}\leftrightarrow-\frac{1}{2})$ transition. H_1-H_5 represent the fields where the powder pattern has a singularity, step or shoulder.

step at H_3. Therefore, in the present case of a constant frequency ν_0, the shift $\delta\nu_j$ ($j=1-3$) defined by the difference between ν_0 and γ^*H_j, where $\gamma^*=\gamma/(2\pi)$ (γ is the nuclear gyromagnetic ratio, $^{63}\gamma=2\pi\times1.1285\times10^3$ and $^{65}\gamma=2\pi\times1.2089\times10^3$ MHz/Oe) is expressed as

$$\frac{\delta\nu_j}{\gamma^*H_j}=K_{jj}+\frac{C_j}{(1+K_{jj})(\gamma^*H_j)^2} \tag{1}$$

with

$$C_1=\frac{R(3+\eta)^2}{144}\ , \tag{2}$$

$$C_2=\frac{R(3-\eta)^2}{144}\ , \tag{3}$$

$$C_3=\frac{R\eta^2}{36}\ , \tag{4}$$

and

$$R=\nu_Q^2[I(I+1)-\tfrac{3}{4}]\ , \tag{5}$$

where ν_Q is the quadrupole frequency, I is the nuclear spin ($I=\frac{3}{2}$ for ^{63,65}Cu), and K_{jj} ($j=1$, 2, and 3) correspond to the X, Y, and Z principal values of the Knight shift tensor, respectively. Therefore, if $\delta\nu_j/(\gamma^*H_j)$ is plotted against $(\gamma^*H_j)^{-2}$, the linear relation is expected. The intersection between the straight line and the vertical axis yields the principal values $K_{\mu\mu}$ ($\mu=X$, Y, and Z) of the Knight shift tensor. Here we should note that the Knight shift can be generally defined only when magnetization is proportional to a magnetic field. Below $T_{\rm sp}$ where an opening of the energy gap takes place in the magnetic excitation spectrum, magnetization is not proportional to a magnetic field. Therefore, the Knight shift measured below $T_{\rm sp}$ is proportional not to the magnetic susceptibility but to the magnetization at the measured field. However, we determined K_{XX} and K_{YY} using $\delta\nu_j/(^{65}\gamma^*H_j)$ vs $(^{65}\gamma^*H_j)^{-2}$ plot in the frequency range 75.5–93 MHz, because a linear M vs H relation is expected to hold in such a frequency range. Indeed, $\delta\nu_1/(^{65}\gamma^*H_1)$ is proportional to $(^{65}\gamma^*H_1)^{-2}$ as shown in Fig. 6. On the other hand, we determined K_{ZZ} by fitting the peak at H_5 and the shoulder at H_6 for ^{63}Cu and ^{65}Cu at 75.5 MHz to Eqs. (A4) and (A5), respectively, because we could not observe the step at H_3 which is usually hard to be observed in comparison with the other peaks and shoulders. Also, we determined ν_Q and η from the slope of the straight line in the $\delta\nu_j/(\gamma^*H_j)$ vs $(\gamma^*H_j)^{-2}$ plot. Thus, for example, it was obtained at 4.2 K that $^{65}\nu_Q=31.41\pm0.10$ ($^{63}\nu_Q=33.95\pm0.11$) MHz, $\eta=0.16\pm0.01$, $K_{XX}=0.37\pm0.02\%$, $K_{YY}=0.34\pm0.03\%$, and $K_{ZZ}=1.76\pm0.03\%$. Furthermore, these values of ν_Q, η, and $K_{\mu\mu}$ were checked by comparing the experimental resonance fields of satellite transitions ($\pm\frac{1}{2}\leftrightarrow\pm\frac{3}{2}$) with calculated ones which are denoted by the solid (^{63}Cu) and dotted (^{65}Cu) arrows in Fig. 5. The obtained EFG parameters are consistent with a low-field NMR result.[20] The experimental values of $K_{\mu\mu}$ show that the Knight shift has an axial anisotropy, namely, $K_\parallel=K_{ZZ}$ and $K_\perp=K_{XX}=K_{YY}$. Here, it should be noted that the principal axes of the Knight shift tensor are not the crystal axes but the local symmetry ones at the Cu sites. The Z axis is estimated to be close to the Cu-O(1) bonding axis in an elongated CuO(1)$_2$O(2)$_4$ octahedron, while the X and Y axes are to the Cu-O(2) bondings. Therefore, it is safe to say that the Cu^{2+} ion in CuGeO$_3$ is located in an octahedral crystal field with a tetragonal symmetry. Also, it should be noted that the directions of the Z axis at the two Cu sites in a unit cell are different from each other.

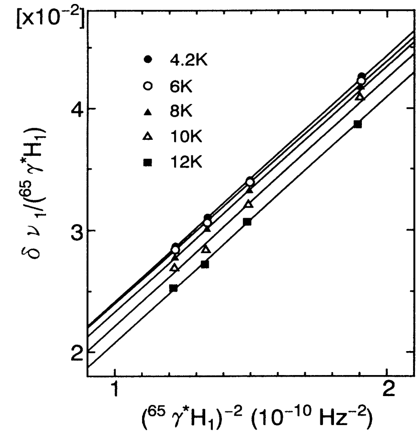

FIG. 6. $\delta\nu_1/(^{65}\gamma^*H_1)$ vs $(^{65}\gamma^*H_1)^{-2}$ plot in CuGeO$_3$ at various temperatures in the frequency range 75.5–93 MHz for the field H_1 where the ^{65}Cu NMR powder spectrum of the central ($\frac{1}{2}\leftrightarrow-\frac{1}{2}$) transition has a peak. $\delta\nu_1$ is the difference between the resonance frequency and $^{65}\gamma^*H_1$.

Figure 7 shows the temperature dependence of the Cu Knight shift $K_{\mu\mu}$ ($\mu=X$, Y, and Z). Below $T_{\rm sp}\sim14$ K, $K_{\mu\mu}$ increases with decreasing temperature and saturates below ~4 K. This temperature dependence is due to the reduction of the spin susceptibility accompanied by the

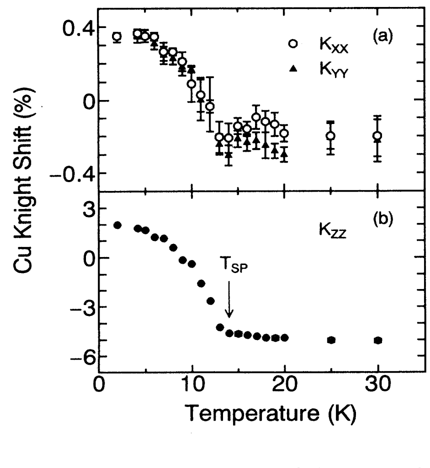

FIG. 7. Temperature dependence of the Cu Knight shifts (a) K_{XX}, K_{YY} and (b) K_{ZZ} in CuGeO$_3$. The X, Y, and Z axes are the principal axes of the Knight shift tensor.

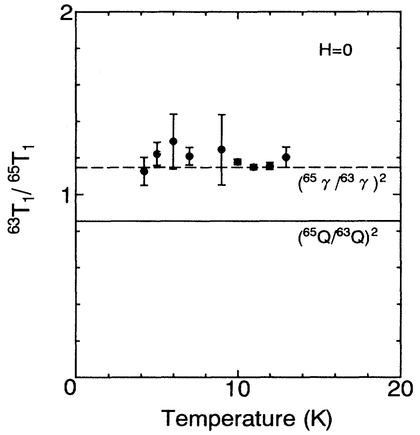

FIG. 8. Temperature dependence of $^{63}T_1/^{65}T_1$ below $T_{\rm sp}$ in CuGeO$_3$. The dashed and solid lines are the relations $^{63}T_1/^{65}T_1=(^{65}\gamma/^{63}\gamma)^2$ and $(^{65}Q/^{63}Q)^2$, respectively, where γ is the nuclear gyromagnetic ratio and Q is the nuclear quadrupole moment.

SP transition. Therefore, the Knight shifts extrapolated at $T=0$ K, $K_{\parallel}=1.95\pm0.03\%$ and $K_{\perp}=0.35\pm0.02\%$, are the orbital shifts $K_{\parallel}^{\rm orb}$ and $K_{\perp}^{\rm orb}$ in the SP phase, respectively. Figures 4(b) and 4(c) show the temperature dependence of ν_Q and η, respectively.

D. Nuclear spin-lattice relaxation time

We measured the nuclear magnetization recovery $P(t)$ by means of the saturation recovery method for the NQR signals in zero external field. A nonexponential recovery of $P(t)$ due to the impurity local moments was observed below ~9 K, whereas we observed an exponential recovery above ~9 K. We determined T_1 by the least-squares fitting $P(t)$ to the sum of two exponential recoveries in which the long-time recovery is considered to be intrinsic. We also compared $^{63}T_1$ with $^{65}T_1$ to clarify whether the origin of the relaxation is magnetic or electric. Figure 8 shows the temperature dependence of $^{63}T_1/^{65}T_1$ below $T_{\rm sp}$ which is equal to the ratio $(^{65}\gamma/^{63}\gamma)^2=1.148$ rather than $(^{65}Q/^{63}Q)^2=0.8558$, showing the magnetic origin. The temperature dependence of $1/^{63}T_1$ is presented in Fig. 9 which is in agreement with the previous report.[19] Below $T_{\rm sp}$, the reduction of $1/T_1$ indicates an appearance of a gap in the magnetic excitation spectrum. Above $T_{\rm sp}$, $1/T_1$ gradually increases concavely upward with increasing temperature. A finite value of $(6.0\pm0.5)\times10^2$ sec^{-1} is extrapolated at $T=0$ K, if the SP transition is removed down to $T=0$ K.

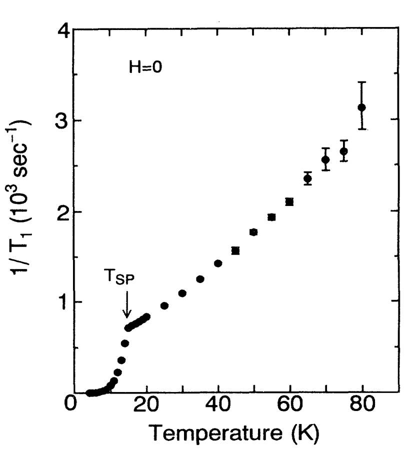

FIG. 9. Temperature dependence of the ^{63}Cu nuclear spin-lattice relaxation rate $1/T_1$ taken for the ^{63}Cu NQR line in CuGeO$_3$.

IV. ANALYSIS AND DISCUSSION

A. NQR frequency and lattice dimerization

No anomaly of ν_Q ($\nu_{\rm NQR}$) was observed in the present experiment. To estimate the variation of ν_Q accompanied by the SP transition, we use an empirical relation between ν_Q and $V_{ZZ}^{\rm lat}$ which was found by Shimizu[28] for Cu^{2+} in various insulating copper oxides. The relation is denoted as $\nu_Q=AV_{ZZ}^{\rm lat}+B$, where A $[=-(16.1\pm0.4)\times10^{-8}$ Hz/esu for ^{63}Cu] and B $(=77.0\pm1.8$ MHz for ^{63}Cu) are the constants independent of materials. Here, the contribution to the EFG from the surrounding lattice ions $V_{ZZ}^{\rm lat}$ is calculated within the point charge model. If the temperature variation of the displacement δu_i^k of each ion [$i=$Cu and O(2), and $k=a$, b, and c] has the form of $\delta u_i^k=(\delta u_i^k)_0(1-T/T_{\rm sp})^\beta$ with

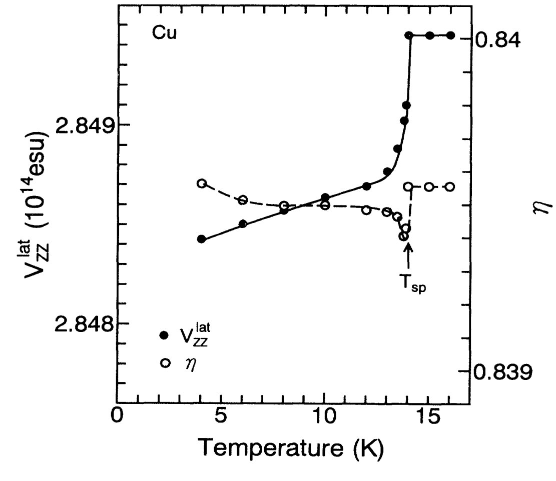

FIG. 10. Temperature dependence of the electric-field gradient $V_{ZZ}^{\rm lat}$ and the asymmetry parameter η due to the surrounding lattice ions in CuGeO$_3$. They are calculated based on a point charge model with taking into account the progressive displacement of each ion accompanied by the SP transition and the temperature variation of the lattice constants. The solid and dashed curves are drawn to guide the eye.

$\beta=0.093$,[18] the temperature dependence of $V_{ZZ}^{\rm lat}$ and η can be calculated by using the temperature-dependent lattice constants[13,25] and the reported displacements.[25] The results are presented in Fig. 10. Based on these results, the temperature variation of ν_Q is estimated as represented by the solid curve in Fig. 4(b). Furthermore, $\nu_{\rm NQR}$ $(=\nu_Q\sqrt{1+\eta^2/3})$ is evaluated as is denoted by the solid curve in Fig. 4(a), assuming a temperature-independent η of 0.16. Thus the difference between $\nu_{\rm NQR}$ (ν_Q) above and below $T_{\rm sp}$ is too small to be detected in the present NQR (NMR) measurement, as can be seen in Fig. 4(a) [4(b)].

B. Orbital susceptibility

Magnetic susceptibility and Knight shift of $3d$ transition-metal oxides are generally expressed as $\chi=\chi^{\rm spin}(T)+\chi^{\rm orb}+\chi^{\rm dia}$ and $K=K^{\rm spin}(T)+K^{\rm orb}$, respectively. Here, $K^{\rm spin}(T)$ and $K^{\rm orb}$ are the Knight shifts due to spin susceptibility $\chi^{\rm spin}(T)$ and orbital susceptibility $\chi^{\rm orb}$, respectively, and $\chi^{\rm dia}$ is diamagnetic susceptibility.

The orbital susceptibility $\chi^{\rm orb}$ of a Cu^{2+} ion in an octahedral crystal field with a tetragonal symmetry can be expressed as

$$\chi_{\parallel}^{\rm orb}=\frac{8N_A\mu_B^2\xi^2}{\Delta_0} \tag{6}$$

and

$$\chi_{\perp}^{\rm orb}=\frac{2N_A\mu_B^2\xi^2}{\Delta_1}\ , \tag{7}$$

where N_A is the Avogadro's number, μ_B is the Bohr magneton, ξ is the orbital reduction factor, Δ_0 is the energy difference between $d_{X^2-Y^2}$ and d_{XY}, and Δ_1 is between $d_{X^2-Y^2}$ and d_{YZ} (d_{ZX}).[29] On the other hand, the Knight shift $K_\alpha^{\rm orb}$ ($\alpha=\parallel$ and $\perp$) due to $\chi_\alpha^{\rm orb}$ is generally expressed as

$$K_\alpha^{\rm orb}=2\langle r^{-3}\rangle_{3d}\chi_\alpha^{\rm orb}\ . \tag{8}$$

The displacements of the Cu and O(2) sites may lead to a slight modification of the Cu^{2+} electronic state by the change of the crystal-field parameters. However, we neglect such an effect on $\chi^{\rm orb}$. At $T\ll T_{\rm sp}$, $K\rightarrow K^{\rm orb}$, because $K^{\rm spin}\rightarrow 0$. Therefore, we can estimate $\chi_\alpha^{\rm orb}$ from the experimental values of $K_\parallel^{\rm orb}=1.95\pm0.03\%$ and $K_\perp^{\rm orb}=0.35\pm0.02\%$ by using the value of $\langle r^{-3}\rangle_{3d}=6.04$ a.u.,[28] which is 73% of the Hartree-Fock value. The values we obtained are $\chi_\parallel^{\rm orb}=(1.44\pm0.02)\times10^{-4}$, $\chi_\perp^{\rm orb}=(0.26\pm0.01)\times10^{-4}$, and $\chi_{\rm iso}^{\rm orb}=(\chi_\parallel^{\rm orb}+2\chi_\perp^{\rm orb})/3=(0.65\pm0.02)\times10^{-4}$ emu/mol. The ratio Δ_1/Δ_0 is also evaluated as 1.38 ± 0.07 from Eqs. (6) and (7).

On the other hand, the ratio of $\Delta_1/\Delta_0=\chi_\parallel^{\rm orb}/4\chi_\perp^{\rm orb}=(2-g_\parallel)/4(2-g_\perp)$ can also be estimated from the g values. The $g_\parallel$ and $g_\perp$ values are expressed as

$$g_\parallel=2-\frac{8\lambda_{\rm so}\xi^2}{\Delta_0} \tag{9}$$

and

$$g_\perp=2-\frac{2\lambda_{\rm so}\xi^2}{\Delta_1}\ , \tag{10}$$

where $\lambda_{\rm so}$ is the coupling parameter of the spin-orbit interaction.[29] Since the principal axes of the g tensor $g_\parallel$ and $g_\perp$ are located in the ab plane, g in the ab plane is calculated as

$$g=\sqrt{g_\parallel^2\cos^2\theta+g_\perp^2\sin^2\theta}\ , \tag{11}$$

where θ is the angle between the Z axis and the external field.[29] From the values of $g_a=2.162\pm0.002$, $g_b=2.266\pm0.002$, and $g_c(=g_\perp)=2.070\pm0.002$ determined by the EPR measurement,[21] $g_\parallel$ and $g_\perp$ values are calculated to be 2.350 ± 0.002 and 2.070 ± 0.002, respectively. Thus, Δ_1/Δ_0 is obtained to be 1.25 ± 0.04, which agrees with the value of 1.38 ± 0.07 determined by the NMR measurement mentioned above.

C. Hyperfine coupling constant

In the present case of the orbital singlet ground state, the Knight shift $K_\alpha^{\rm spin}$ due to the spin susceptibility $\chi_\alpha^{\rm spin}$ is expressed as

$$K_\alpha^{\rm spin}=A_\alpha\chi_\alpha^{\rm spin}\ . \tag{12}$$

The total hyperfine coupling constant A_α is expressed as

$$A_\alpha=A^{\rm Fermi}+A_\alpha^{\rm orb}+A_\alpha^{\rm so}\ , \tag{13}$$

where $A^{\rm Fermi}$, $A_\alpha^{\rm dip}$, and $A_\alpha^{\rm so}$ are the Fermi contact, dipole, and spin-orbit hyperfine coupling constants, respectively. For a Cu^{2+} ion in a tetragonal symmetry, $A_\alpha^{\rm dip}$ and $A_\alpha^{\rm so}$ are written as[29]

$$A_\parallel^{\rm dip}=-2A_\perp^{\rm dip}=-\tfrac{4}{7}\langle r^{-3}\rangle_{3d}\ , \tag{14}$$

$$A_\parallel^{\rm so}=-\frac{11\lambda_{\rm so}\xi^2}{7\Delta_1}\langle r^{-3}\rangle_{3d}\ , \tag{15}$$

and

$$A_\perp^{\rm so}=-\left[\frac{8\lambda_{\rm so}\xi^2}{\Delta_0}+\frac{6\lambda_{\rm so}\xi^2}{7\Delta_1}\right]\langle r^{-3}\rangle_{3d}\ . \tag{16}$$

From Eq. (12), it is found that the K_α vs χ_α plot with temperature as an implicit parameter yields A_α. Instead, in Fig. 11, we show the isotropic Knight shift $K_{\rm iso}$ vs $M/H-\chi_{\rm dia}$ plot [$\chi_{\rm dia}=-5.4\times10^{-5}$ emu/mol (Ref. 30)] where M is the magnetization at $H=5$ T and M/H above $T_{\rm sp}$ is equal to $\chi_{\rm iso}$, because the χ_α data of CuGeO$_3$ are not available. As can be seen in Fig. 11, the data below 14 K deviate from the linear relation between $K_{\rm iso}$ and $M/H-\chi_{\rm dia}$ found above 15 K. The deviation below $T_{\rm sp}$ seems to be closely correlated to the SP transition. However, we will not discuss the deviation at present because of lack of sufficient information. Nevertheless, we can reasonably discuss the hyperfine structure based on the data above $T_{\rm sp}$ of the $K_{\rm iso}$ vs $M/H-\chi_{\rm dia}$ plot. We also present the $K_\parallel$ vs $K_\perp$ plot with temperature as an implicit parameter in Fig. 12. A linear relation, $K_\parallel=11.6K_\perp-2.28\times10^{-2}$, holds between $K_\parallel$ and $K_\perp$,

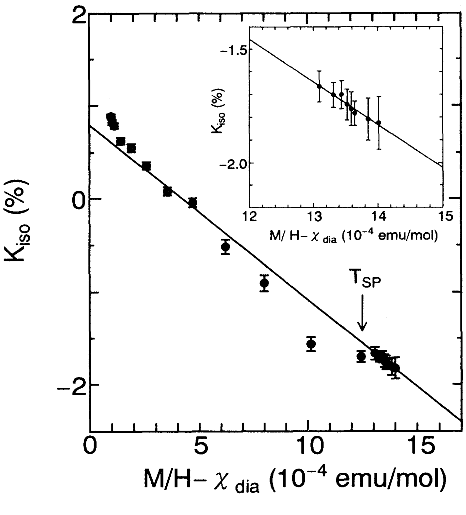

FIG. 11. K_{iso} vs $M/H-\chi_{dia}$ plot with temperature as an implicit parameter for the Cu isotropic Knight shift in CuGeO$_3$. M is the magnetization at $H=5$ T, and χ_{dia} is the diamagnetic susceptibility. The inset is an expanded figure above 15 K. The solid lines represent the best fit of the data above 15 K to a linear relation between K_{iso} and $M/H-\chi_{dia}$.

TABLE I. Values of hyperfine coupling constants above T_{sp} in CuGeO$_3$. For comparison, values in CuO and YBa$_2$Cu$_3$O$_7$ are listed. Units are in kOe/μ_B.

	CuGeO$_3$	CuO[a]	YBa$_3$Cu$_3$O$_{7-\delta}$[b]
$A_\parallel$	-268 ± 12	-146 ± 10	-22.2 ± 0.2
$A_\perp$	-23 ± 5	15 ± 15	128 ± 1
A^{Fermi}	-143 ± 7	-125 ± 15	28 ± 4
$A_\parallel^{\text{dip}}$	-216 ± 6	-225 ± 6	-168 ± 4
$A_\perp^{\text{dip}}$	108 ± 3	112 ± 3	84 ± 2
$A_\parallel^{\text{so}}$	91 ± 17	203 ± 20	117 ± 5
$A_\perp^{\text{so}}$	12 ± 2	27.4 ± 5.0	17 ± 5

[a] Reference 31.
[b] Reference 32.

which means that $dK_\parallel/dT=dK_\perp/dT=dK_{iso}/dT$, namely, $d\chi_\parallel/dT=d\chi_\perp/dT=d\chi_{iso}/dT$. Therefore, we can write

$$\frac{dK_{iso}/dT}{d\chi_{iso}/dT}=\frac{2}{3}A_\perp^{\text{spin}}+\frac{1}{3}A_\parallel^{\text{spin}} \tag{17}$$

and

$$\frac{dK_\parallel/dT}{dK_\perp/dT}=\frac{A_\parallel^{\text{spin}}}{A_\perp^{\text{spin}}} . \tag{18}$$

Using the experimental values of $dK_{iso}/d\chi_{iso}=-105\pm7$ kOe/μ_B above 15 K and $dK_\parallel/dK_\perp=11.6\pm0.3$, $A_\parallel^{\text{spin}}$ and $A_\perp^{\text{spin}}$ listed in Table I are obtained. Furthermore, A_α^{spin} can be divided into A^{Fermi}, A_α^{dip}, and A_α^{so} as summarized in Table I where the CuO (Ref. 31) and YBa$_2$Cu$_3$O$_{7-\delta}$ (Ref. 32) data analyzed based on the same crystal field are also listed for comparison. We note that each component of A_α^{spin} estimated for CuGeO$_3$ is reasonably explained within this single-ion model as can be seen in comparison with those of CuO having a typical single-ion character. However, CuGeO$_3$ is remarkably different from the high-T_c superconductor where A^{Fermi} at the plane Cu sites is positive due to the strong hybridization between the p_σ orbital of O^{2-} and the $3d_{X^2-Y^2}$ and $4s$ orbitals of Cu^{2+}.[33] The presence of this supertransferred hyperfine mechanism is strongly dependent on the Cu$_{(1)}$-O(2)-Cu$_{(2)}$ bonding angle θ_a. In CuGeO$_3$, $\theta_a\sim100°$,[16] resulting in a very small overlap between the p_σ orbital, which mixes into the $d_{X^2-Y^2}$ orbital of the Cu$_{(1)}$ ion, and the 4s orbital of the Cu$_{(2)}$ ion, while $\theta_a\sim180°$ for the plane Cu sites in YBa$_2$Cu$_3$O$_{7-\delta}$. This is the main reason for the absence of the supertransferred hyperfine interaction in CuGeO$_3$.

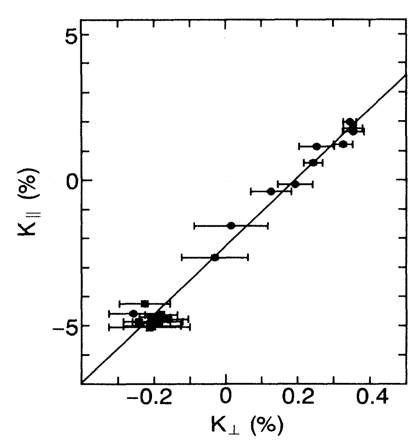

FIG. 12. $K_\parallel$ vs $K_\perp$ plot temperature as an implicit parameter for the Cu Knight shifts in CuGeO$_3$. The solid line represents a relation $K_\parallel=11.6K_\perp-2.28\times10^{-2}$.

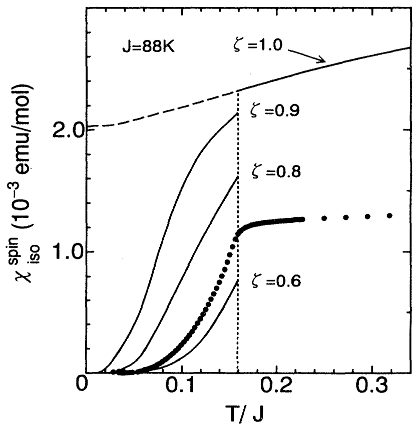

FIG. 13. Temperature dependence of the isotropic spin susceptibility χ_{iso}^{spin} of CuGeO$_3$. The solid curves are the theoretical ones on the $S=\frac{1}{2}$ 1DHAF with the two unequal alternating exchange interactions J_1 and J_2 ($J_1>J_2$) for various $\zeta=J_2/J_1$ (after Ref. 34). The $\zeta=1$ curve corresponds to a numerical result by Bonner and Fisher of the $S=\frac{1}{2}$ DHAF with $J=88$ K.

D. Spin susceptibility

From the Knight shift data mentioned above, we estimate the temperature dependence of the isotropic spin susceptibility $\chi_{\mathrm{iso}}^{\mathrm{spin}}$ as is shown in Fig. 13. We compare the temperature dependence of $\chi_{\mathrm{iso}}^{\mathrm{spin}}$ below T_{sp} with the theoretical curves for the 1DHAF with two alternating antiferromagnetic exchange interactions J_1 and J_2 ($J_1 \geq J_2$), which were obtained by extrapolating the exact calculations up to 12 spins to the infinite chain for various $\zeta = J_2/J_1$.[34] With the progressive dimerization in the SP phase, ζ must have such temperature dependence as $\zeta \to 1$ with $T \to T_{\mathrm{sp}}$.[1] However, the theoretical $\chi_{\mathrm{iso}}^{\mathrm{spin}}$ vs T curves fail to reproduce the observed temperature dependence of $\chi_{\mathrm{iso}}^{\mathrm{spin}}$ in CuGeO$_3$ as can be seen in Fig. 13. Also, above T_{sp}, there exists the discrepancy between the Bonner-Fisher curve with $J = 88$ K and the experimental $\chi_{\mathrm{iso}}^{\mathrm{spin}}$. These features of $\chi_{\mathrm{iso}}^{\mathrm{spin}}$ are remarkably different from those of the other organic SP compounds where $\chi_{\mathrm{iso}}^{\mathrm{spin}}$ is well explained by the 1DHAF model.[1] At present, we cannot find the origin of the discrepancy.

E. Spin dynamics

Nuclear spin-lattice relaxation rate $1/T_1$ is powerful to study the low-lying magnetic excitation spectrum.

First, we will discuss the temperature dependence of $1/T_1$ above T_{sp} based on the $S=\frac{1}{2}$ 1DHAF model for which the nuclear relaxation has been treated by the spinless fermion[35,36] and slave fermion mean-field[37] theories. The relaxation studies based on the spinless fermion by Ehrenfreund *et al.*[35,36] have been successful in explaining $1/T_1$ at low temperatures of the organic salts N-methyl phenazinium tetracyanoquinodimethan (NMP-TCNQ), TTF-AuBDT, and TTF-CuBDT. Within the spinless fermion theory,[35,36] at $k_B T \ll J$, $1/T_1$ is expressed as

$$\frac{1}{T_1} = \frac{(A_{\perp}^{\mathrm{spin}})^2}{2\hbar J p(T)} \tag{19}$$

with

$$p(T) \simeq \left[1 + \frac{2}{\pi}\right]\left[1 - \frac{\pi}{3(1+2/\pi)^3}\left[\frac{k_B T}{J}\right]^2 + \cdots\right]. \tag{20}$$

Therefore, $1/T_1$ is approximately expressed as $1/T_1 = a_0 + b_0 T^2$ at $k_B T \ll J$. In CuGeO$_3$, a_0 and b_0 are calculated to be 2.09×10^3 sec^{-1} and 3.46×10^{-2} sec^{-1}K^{-2}, respectively, using experimental values of $A_{\perp}^{\mathrm{spin}} = -23$ kOe/μ_B and $J = 120.4$ K (10.4 meV). The calculated a_0 is a factor of 3 larger than the experimental value of $(6.0 \pm 0.5) \times 10^2$ sec^{-1}, and the calculated temperature dependence of $1/T_1$ does not agree with the experimental data in the temperature range 15–80 K ($<J$) as is seen in Fig. 14. Therefore, the spinless fermion treatment fails to explain the nuclear relaxation in CuGeO$_3$, which indicates that the Hartree-Fock approximation for the interaction between fermions is poor. This failure is not removed by the slave fermion mean-field theory, which was developed by Cox and Trees[37] to explain the temperature variation of $1/T_1$ at the Cu(1) chain site in a high-T_c superconducting copper oxide YBa$_2$Cu$_3$O$_{7-\delta}$, as shown in Fig. 14 where the dashed curve represents the slave fermion result.

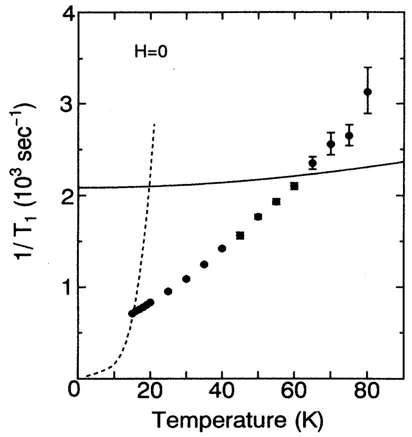

FIG. 14. Calculated temperature dependence of the nuclear spin-lattice relaxation rate $1/T_1$ for the 1DHAF model of $S=\frac{1}{2}$. The solid and dashed curves are based on the spinless fermion and the slave fermion mean-field (after Ref. 37) theories, respectively (see the text). The solid circles are the experimental data of $1/T_1$ above T_{sp} taken for the ^{63}Cu NQR line in CuGeO$_3$.

Next, we will consider the dynamical susceptibility of the $S=\frac{1}{2}$ 1DHAF model to discuss further the temperature dependence of $1/T_1$ above T_{sp} beyond the mean-field theories. In general, $1/T_1T$ is related to the transverse dynamical susceptibility $\chi^{+-}(q,\omega)$ as

$$\frac{1}{T_1 T} = \frac{\gamma^2 k_B}{2\mu_B^2}(A_{\perp}^{\mathrm{spin}})^2 \sum_q \frac{\mathrm{Im}\chi^{+-}(q,\omega_n)}{\omega_n}, \tag{21}$$

where ω_n is the nuclear Larmor frequency. The temperature dependence of $1/T_1T$ in CuGeO$_3$ is shown in Fig. 15. In the $S=\frac{1}{2}$ 1DHAF model, the q summation over the Brillouin zone in Eq. (21) is dominated by $q=0$ and π where the energy gap is absent in the excited spectrum. Therefore, $1/T_1T$ has two contributions from $q=0$, $(1/T_1T)_{q=0}$ and $q=\pi$, $(1/T_1T)_{q=\pi}$. Recently, Schulz[38] calculated the dynamical correlation function $S^{\mu\mu}(q,\omega)$ by mapping the 1DHAF Hamiltonian onto a relativistic quantum field theory and exploiting the bosonization method[39] of Luther and Peschel. He obtained an analytical expression of $S^{\mu\mu}(q,\omega)$ near $q=\pi$ as

$$S^{\mu\mu}(q,\omega) \propto (n_\omega + 1)\,\mathrm{Im}\left[\frac{1}{T}\rho\left[\frac{\omega - vQ}{4\pi k_B T}\right]\rho\left[\frac{\omega + vQ}{4\pi k_B T}\right]\right] \tag{22}$$

with

$$\rho(x) = \frac{\Gamma(\frac{1}{4} - ix)}{\Gamma(\frac{3}{4} - ix)}, \tag{23}$$

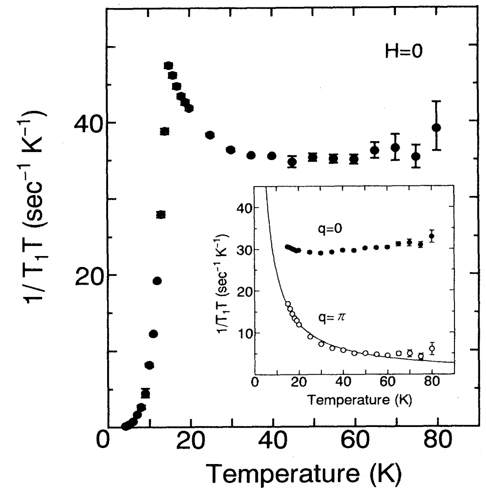

FIG. 15. Temperature dependence of $1/T_1T$ where T_1 is the ^{63}Cu nuclear spin-lattice relaxation time taken for the NQR line in CuGeO$_3$. The inset shows the temperature dependence of the $q=0$ contribution to $1/T_1T$, $(1/T_1T)_{q=0}$, and the $q=\pi$ contribution, $(1/T_1T)_{q=\pi}$. The solid curve represents a theoretical one for $(1/T_1T)_{q=\pi}$.

where $Q=q-\pi$, $v=\pi J$, n_ω is the Bose factor, and Γ is the gamma function.[38,40,41] Thus, we obtain $(1/T_1T)_{q=\pi}$, which is proportional to $1/T$, by inserting $\mathrm{Im}\chi^{+-}(q,\omega)=S^{+-}(q,\omega)/(n_\omega+1)$ to Eq. (21). The solid curve in the inset of Fig. 15 is the best fit to the $1/T$ dependence. On the other hand, $(1/T_1T)_{q=0}$ is estimated by subtracting $(1/T_1T)_{q=\pi}$ from the experimental $1/T_1T$ data as is also shown in Fig. 15. This calculation seems to explain the observed temperature dependence of $1/T_1T$ above $T_{\rm sp}$ in CuGeO$_3$.

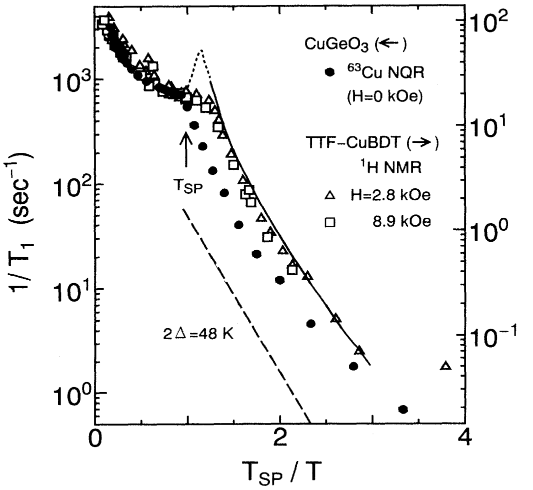

FIG. 16. $1/T_1$ vs $T_{\rm sp}/T$ plot in CuGeO$_3$ ($T_{\rm sp}=14$ K) and TTF-CuBDT ($T_{\rm sp}=12$ K, after Ref. 42). The nuclear spin-lattice relaxation time T_1 was measured for the ^{63}Cu NQR line in CuGeO$_3$ and for the ^{1}H NMR line in TFF-CuBDT. The CuGeO$_3$ data denoted by the solid circles refer to the left vertical axis, while the TTF-CuBDT data represented by the open triangles and squared refer to the right axis. The solid ($T<0.75T_{\rm sp}$) and dotted ($0.75T_{\rm sp}<T<T_{\rm sp}$) curve represents a theoretical one calculated by Ehrenfreund and Smith for a nonuniform Heisenberg $S=\frac{1}{2}$ chain with two unequal and alternating exchange interactions. The dashed line is proportional to $\exp(-2\Delta/k_BT)$ with $\Delta/k_B=24$ K.

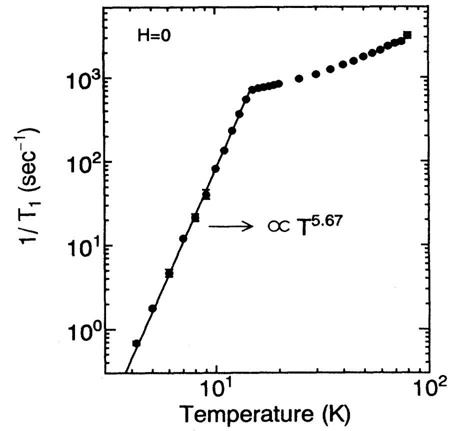

FIG. 17. $\log(1/T_1)$ vs $\log(T)$ plot in CuGeO$_3$. The nuclear spin-lattice relaxation time T_1 was measured for the ^{63}Cu NQR line in zero magnetic field. The solid line is the best fit to a relation $1/T_1 \propto T^n$ below $T_{\rm sp}$.

Now, we will discuss the temperature dependence of $1/T_1$ below $T_{\rm sp}$. The system can be treated as a nonuniform Heisenberg $S=\frac{1}{2}$ spin chain with two unequal and alternating exchange constants. Ehrenfreund and Smith[42] described the model as a system of interacting fermions distributed in two bands with a minimum energy gap in the excitation spectrum. For the $1/T_1$ mechanism, they proposed an indirect process in the lowest order accompanied by three excitations because the direct process is forbidden. As is represented by the dotted curve in Fig. 16, the theoretical $1/T_1$ is enhanced just below $T_{\rm sp}$ due to the singularity of the density of states. However, the enhancement is reduced by taking account of a finite broadening of the excitation energies. Below $0.75T_{\rm sp}$, $1/T_1$ shows a temperature dependence represented by the solid curve in Fig. 16. At low temperatures $T \ll \Delta(T)/k_B$, $1/T_1$ is proportional to $\exp(-2\Delta/k_BT)$. As is shown in Fig. 16, the proton relaxation data in an organic SP compound TTF-CuBDT were explained by their theory. In CuGeO$_3$, however, the T variation of $1/T_1$ is weaker than $\exp(-2\Delta/k_BT)$ with $\Delta(T=0)/k_B=24$ K (Refs. 4 and 18) at $T \ll T_{\rm sp}$, and is better traced by $T^{5.67\pm0.03}$ in the temperature range from just below $T_{\rm sp}$ to 4.2 K as is shown in Fig. 17. Therefore, this relaxation mechanism is not successful in explaining the nuclear relaxation below $T_{\rm sp}$ in CuGeO$_3$. Further theoretical investigations are required to understand the temperature dependence of $1/T_1$ below $T_{\rm sp}$ in CuGeO$_3$.

V. CONCLUSIONS

We have performed ^{63,65}Cu NQR and NMR measurements to probe the Cu^{2+} electronic state and the spin dynamics in the SP compound CuGeO$_3$. The change accompanied by the SP transition in the electric-field gradient parameters was found to be very small, and was not observed in the present study. We observed the anisotropic Knight shift with an axial symmetry. Below T_{sp} the Knight shift varies with temperature accompanied by the decreases in spin susceptibility. From the analysis of the Knight shift and the magnetic susceptibility, the Cu^{2+} electronic state was found to be described by a single-ion model in an octahedral crystalline field with a tetragonal symmetry. The temperature dependence of the nuclear spin-lattice relaxation rate $1/T_1$ clearly showed an appearance of the gap in the magnetic excitation spectrum below T_{sp}. However, the spin dynamics could not be explained by the spinless fermion treatments in both uniform and SP phases. It was shown that the $1/T_1$ above T_{sp} provides useful information on the dynamical susceptibility in the 1DHAF.

ACKNOWLEDGMENTS

The authors would like to thank H. Yasuoka, H. Ohta, and J. Kikuchi for fruitful discussions, and S. Tsuda, M. Sugahara, and Y. Nishimaki for their experimental assistance. This study was partly supported by the Futaba Electronics Memorial Foundation.

APPENDIX

If the quadrupole effect is treated up to the second order of the perturbation for the Zeeman interaction, locations of shoulders and singularities in the powder pattern for the central $(+\frac{1}{2}\leftrightarrow-\frac{1}{2})$ transition are expressed as[27]

$$\nu_1=\nu_0+\frac{R(3+\eta)^2}{144\nu_0}+K_{XX}\nu_0\ , \tag{A1}$$

$$\nu_2=\nu_0+\frac{R(3-\eta)^2}{144\nu_0}+K_{YY}\nu_0\ , \tag{A2}$$

$$\nu_3=\nu_0+\frac{R\eta^2}{36\nu_0}+K_{ZZ}\nu_0\ , \tag{A3}$$

$$\begin{aligned}\nu_4=\nu_0&-\frac{R(1-\eta)}{9\nu_0}+\frac{(5-\eta)K_{ZZ}+2(2-\eta)K_{XX}}{3(3-\eta)}\nu_0\\&-\frac{4(K_{ZZ}-K_{XX})^2\nu_0^3}{(3-\eta)^2R}\ ,\end{aligned} \tag{A4}$$

and

$$\begin{aligned}\nu_5=\nu_0&-\frac{R(1+\eta)}{9\nu_0}+\frac{(5+\eta)K_{ZZ}+2(2+\eta)K_{YY}}{3(3+\eta)}\nu_0\\&-\frac{4(K_{ZZ}-K_{YY})^2\nu_0^3}{(3+\eta)^2R}\ .\end{aligned} \tag{A5}$$

---

[1] For a review, see J. W. Bray, L. V. Interrante, I. S. Jacobs, and J. C. Bonner, in *Extended Linear Chain Compounds*, edited by J. S. Miller (Plenum, New York, 1983), Vol. 3, p. 353.
[2] F. D. M. Haldane, Phys. Rev. Lett. **50**, 1153 (1983).
[3] J. des Cloizeaux and J. J. Pearson, Phys. Rev. **128**, 2131 (1962).
[4] M. Hase, I. Terasaki, and K. Uchinokura, Phys. Rev. Lett. **70**, 3651 (1993).
[5] M. Hase, I. Terasaki, K. Uchinokura, M. Tokunaga, N. Miura, and H. Obara, Phys. Rev. B **48**, 9616 (1993).
[6] M. Hase, I. Terasaki, Y. Sasago, K. Uchinokura, and H. Obara, Phys. Rev. Lett. **71**, 4059 (1993).
[7] H. Hori, M. Furusawa, T. Takeuchi, S. Sugai, K. Kindo, and A. Yamagishi, J. Phys. Soc. Jpn. **63**, 18 (1994).
[8] T. Hamamoto, N. Adachi, G. Kido, M. Hase, Y. Sasago, and K. Uchinokura, J. Phys. Soc. Jpn. **63**, 1218 (1994).
[9] H. Kuroe, T. Sekine, M. Hase, Y. Sasago, K. Uchinokura, H. Kojima, I. Tanaka, and Y. Shibuya, Phys. Rev. B **50**, 16 468 (1994).
[10] M. Arai, M. Fujita, K. Ubukata, T. Bokui, K. Tabata, H. Ohta, M. Motokawa, T. Otomo, K. Ohyama, M. Mino, J. Akimitsu, and O. Fujita, J. Phys. Soc. Jpn. **63**, 1661 (1994).
[11] M. Nishi, J. Phys. Condens. Matter **6**, L19 (1994).
[12] J. E. Lorenzo, K. Hirota, G. Shirane, J. M. Tranquada, M. Hase, K. Uchinokura, H. Kojima, I. Tanaka, and Y. Shibuya, Phys. Rev. B **50**, 1278 (1994).
[13] S. Katano, H. Nakata, J. Akimitsu, F. Izumi, and M. Nishi (unpublished).
[14] T. M. Brill, J. P. Boucher, J. Voiron, G. Dhalenne, A. Revcolevschi, and J. P. Renard, Phys. Rev. Lett. **73**, 1545 (1994).
[15] L. F. Mattheiss, Phys. Rev. B **49**, 14 050 (1994).
[16] H. Völlenkle, A. Wittmann, and H. Nowotny, Monatsh. Chem. **98**, 1352 (1967).
[17] J. C. Bonner and M. E. Fisher, Phys. Rev. **135**, A640 (1964).
[18] M. Nishi, O. Fujita, and J. Akimitsu, Phys. Rev. B **50**, 6508 (1994).
[19] J. Kikuchi, H. Yasuoka, M. Hase, Y. Sasago, and K. Uchinokura, J. Phys. Soc. Jpn. **63**, 872 (1994).
[20] K. Le Dang, G. Dhalenne, J. P. Renard, A. Revcolevschi, and P. Veillet, Solid State Commun. **91**, 927 (1994).
[21] S. Oseroff, S. W. Cheong, A. Fondado, B. Aktas, and Z. Fisk, J. Appl. Phys. **75**, 6819 (1994).
[22] H. Ohta, S. Imagawa, H. Ushiroyama, M. Motokawa, O. Fujita, and J. Akimitsu, J. Phys. Soc. Jpn. **63**, 2870 (1994).
[23] J. P. Pouget, L. P. Regnault, M. Ain, B. Hennion, J. P. Renard, P. Veillet, G. Dhalenne, and A. Revcolevschi, Phys. Rev. Lett. **72**, 4037 (1994).
[24] O. Kamimura, M. Terauchi, M. Tanaka, O. Fujita, and J. Akimitsu, J. Phys. Soc. Jpn. **63**, 2467 (1994).
[25] K. Hirota, D. E. Cox, J. E. Lorenzo, G. Shirane, J. M. Tranquada, M. Hase, K. Uchinokura, H. Kojima, Y. Shibuya, and I. Tanaka, Phys. Rev. Lett. **73**, 736 (1994).
[26] G. H. Fuller, J. Phys. Chem. Ref. Data **5**, 835 (1976).
[27] J. F. Baugher, P. C. Taylor, T. Oja, and P. J. Bary, J. Chem. Phys. **50**, 4914 (1969).
[28] T. Shimizu, J. Phys. Soc. Jpn. **62**, 772 (1993).
[29] A. Abragam and B. Bleaney, *Electron Paramagnetic Resonance of Transition Ions* (Clarendon, Oxford, 1970).
[30] *Atomic and Molecular Physics,* edited by K. H. Hellwege and A. M. Hellwege, Landolt-Börnstein, New Series, Group II (Springer, Berlin, 1986), Vol. 16.
[31] T. Shimizu, H. Yasuoka, T. Tsuda, K. Koga, and Y. Ueda, Bull. Magn. Res. **12**, 39 (1990).
[32] T. Shimizu, H. Aoki, H. Yasuoka, T. Tsuda, Y. Ueda, K.

Yoshimura, and K. Kosuge, J. Phys. Soc. Jpn. **62**, 3710 (1993).

[33] F. Mila and T. M. Rice, Physica C **157**, 561 (1989).

[34] J. C. Bonner, H. W. J. Blöte, J. W. Bray, and I. S. Jacobs, J. Appl. Phys. **50**, 1810 (1979).

[35] E. Ehrenfreund, E. F. Rybaczewski, A. F. Garito, A. J. Heeger, and P. Pincus, Phys. Rev. B **7**, 421 (1973).

[36] L. S. Smith, E. Ehrenfreund, A. J. Heeger, L. V. Interrante, J. W. Bray, H. R. Hart, Jr., and I. S. Jacobs, Solid State Commun. **19**, 377 (1976).

[37] D. L. Cox and B. R. Trees, Phys. Rev. B **41**, 11 260 (1990).

[38] H. J. Schulz, Phys. Rev. B **34**, 6372 (1986).

[39] A. Luther and I. Peschel, Phys. Rev. B **9**, 2911 (1974).

[40] D. A. Tennant, T. G. Perring, R. A. Cowley, and S. E. Nagler, Phys. Rev. Lett. **70**, 4003 (1993).

[41] R. A. Cowley, D. A. Tennant, T. G. Perring, S. E. Nagler, and A. M. Tsvelik, Physica A **194**, 280 (1993).

[42] E. Ehrenfreund and L. S. Smith, Phys. Rev. B **16**, 1870 (1977).